

# **Molecular Simulation**



ISSN: (Print) (Online) Journal homepage: https://www.tandfonline.com/loi/gmos20

# Inverse design of compression-induced solid – solid transitions in colloids

Chrisy Xiyu Du , Greg van Anders , Julia Dshemuchadse , Paul M. Dodd & Sharon C. Glotzer

**To cite this article:** Chrisy Xiyu Du , Greg van Anders , Julia Dshemuchadse , Paul M. Dodd & Sharon C. Glotzer (2020): Inverse design of compression-induced solid – solid transitions in colloids, Molecular Simulation, DOI: <u>10.1080/08927022.2020.1798005</u>

To link to this article: <a href="https://doi.org/10.1080/08927022.2020.1798005">https://doi.org/10.1080/08927022.2020.1798005</a>







# Inverse design of compression-induced solid - solid transitions in colloids

Chrisy Xiyu Du<sup>a,b</sup>, Greg van Anders <sup>©</sup> <sup>a,c</sup>, Julia Dshemuchadse <sup>©</sup> <sup>d,e</sup>, Paul M. Dodd<sup>d</sup> and Sharon C. Glotzer<sup>a,d,f,g</sup>

<sup>a</sup>Department of Physics, University of Michigan, Ann Arbor, MI, USA; <sup>b</sup>John A. Paulson School of Engineering and Applied Sciences, Harvard University, Cambridge, MA, USA; <sup>c</sup>Department of Physics, Engineering Physics & Astronomy, Queen's University, Kingston, Canada; <sup>d</sup>Department of Chemical Engineering, University of Michigan, Ann Arbor, MI, USA; <sup>e</sup>Department of Materials Science and Engineering, Cornell University, Ithaca, NY, USA; <sup>f</sup>Department of Materials Science and Engineering, University of Michigan, Ann Arbor, MI, USA; <sup>g</sup>Biointerfaces Institute, University of Michigan, Ann Arbor, MI, USA

#### **ABSTRACT**

Ongoing developments in colloidal particle synthesis show promise for using colloids as building blocks for reconfigurable, functional materials, but their rational design remains a challenge. Recent efforts to inversely design a colloidal particle from a self-assembled target structure at a single state point have proven successful even for complex colloidal crystals, replacing trial-and-error searches. Can such approaches be used to design a particle capable of assembling into multiple target structures under multiple conditions, thereby designing a reconfigurable colloidal crystal? Here we present a computational approach for the design of colloids that exhibit distinct target behaviours under different thermodynamic conditions. By extending the digital alchemy inverse design framework to multiple state points, we design hard particle shapes that entropically self-assemble two different colloidal crystal structures at two different densities; upon a small density change, the system reliably reconfigures between the two solids. We also find that the optimal shape satisfying two constraints is not simply an average of the two optimal shapes from each state point, and therefore is not easily intuited.

#### ARTICLE HISTORY

Received 2 March 2020 Accepted 28 June 2020

#### **KEYWORDS**

Inverse design; self-assembly; Monte Carlo simulation; solid–solid transition; colloids

#### 1. Introduction

A central challenge for materials science is the rational design of functional materials. The development of functional materials from colloidal matter [1] has been advanced through new synthesis techniques that yield building blocks which, due to anisotropic shape or interaction patchiness, are candidates for colloidal materials with novel morphologies or properties [2-13]. However, the emergent nature of structural order in colloids [14] means that designing for the structure of a colloidal material, let alone its function, is a challenge. Recent progress has been made for the inverse design of particles for target crystal structures using a variety of techniques [15-19]. These techniques solve the crystal structure inverse design problem by determining a colloidal building block that exhibits one target behaviour, e.g. self-assembly into the tar- get structure, under some prescribed condition. In contrast, designing a material function requires finding building blocks that exhibit multiple target behaviours under a prescribed set of conditions.

Here we present a design framework that couples multiple extended thermodynamic ensembles via the approach of 'digital alchemy' [15,16,20] to design colloidal building blocks that exhibit multiple target behaviours under different thermodynamic conditions. Motivated by simulations [21,22] and experiments [23–27] demonstrating that solid–solid phase transitions (e.g. face-centered cubic cF4-Cu (FCC) $\leftrightarrow$ body-centered cubic cI2-W (BCC), or BCC $\leftrightarrow$ simple cubic cP1-Po (SC)) can occur in colloidal systems under a range of circumstances, here we seek to design solid–solid transitions in colloids. By performing computer simulations in which the shapes of anisotropic colloids are dictated by

two distinct target structures at different densities (see Figure 1), we design particles to undergo nine different solid-solid transitions (see Table 1) *in silico* between the two structures in a

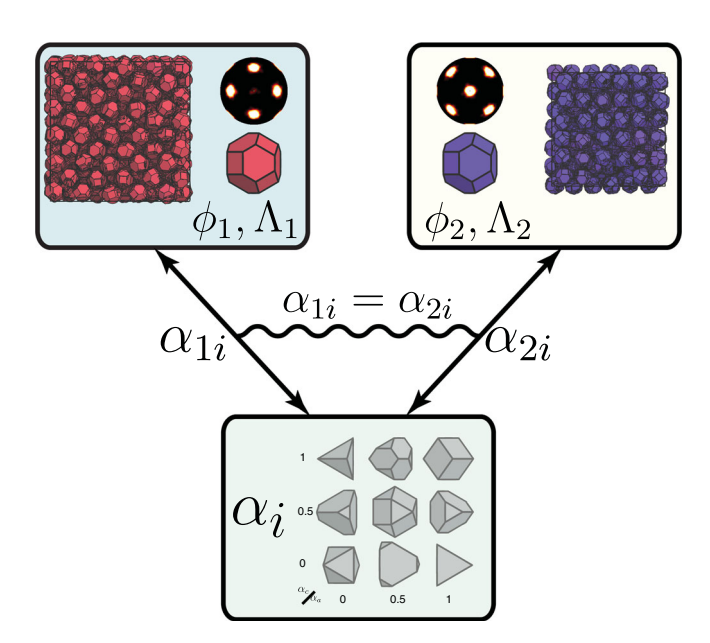


**Figure 1.** (Colour online) The simulation protocol, containing two simulation boxes with different crystal structures ( $\Lambda_1$  and  $\Lambda_2$ ) and different densities ( $\varphi_1$  and  $\varphi_2$ ). Here, the two structures illustrated in the figure are FCC (red) and BCC (blue). Both simulation boxes are subjected to the same 'shape bath' (shape attributes are denoted as  $\alpha_i$ ), where they can interact with each other and make synchronous moves in shape space with different constraints. Shapes illustrated in the figure are subjected to spheric triangle group  $\Delta_{332}$  [28].

Table 1. List of all the transitions studied for this project and our level of success.

Transition	Density Differences	Shape Restrictions	Success
FCC↔BCC	0.55↔0.60 (0.65)	$\Delta_{332}$ , $\Delta_{432}$ , 32, 64 vertices	Stable, Transitions
FCC↔β-Mn	0.55↔0.60 (0.65)	$\Delta_{332}$ , 32, 64 vertices	Stable
FCC↔y-Brass	0.55↔0.60 (0.65)	32, 64 vertices	Stable
FCC↔β-W	0.55↔0.60 (0.65)	32, 64 vertices	Stable
BCC↔SC	0.55↔0.60 (0.65, 0.70)	$\Delta_{332}$ , $\Delta_{432}$ , 32, 64 vertices	Stable, Transitions
BCC <i>⇔cl</i> 16	0.55↔0.60 (0.65, 0.70), 0.60↔0.70	$\Delta_{332}$ , 32, 64 vertices	Stable
BCC↔β-W	0.55↔0.60 (0.65)	32, 64 vertices	Unstable
BCC↔y-Brass	0.55↔0.60 (0.65), 0.60↔0.65	32, 64 vertices	Unstable
FCC↔BCC↔SC	0.55↔0.60↔0.70	$\Delta_{432}$	Stable

prescribed density range. Not every attempt was successful, confirming our expectations that design for behaviours is more challenging than designing for a single structure. By attempting to design transitions that include both simple and complex structures, we explore the limitations of this proposed inverse design method, hoping to provide insights for future improvements. We also show that obtaining the optimal particle shape for a coupled system is not a simple average of the optimal shapes obtained from the individual phases. Although we demonstrate this design approach using hard shapes that self-assemble into colloidal crystals solely by entropy maximisation, the methods we present are easily generalisable to include interparticle interactions of any type.

# 2. Method and model

To design for a colloidal material capable of a density-induced solid-solid phase transition, we must thermodynamically optimise particle attributes-alchemical dimensions-in two different solids simultaneously. The general optimisation framework is that of 'digital alchemy' [15], where the partition function is generalised to include alchemical variables (here: shape):

$$Z = \sum_{i} e^{-\beta \left(H - \sum_{i} \mu_{i} N \alpha_{i} - \lambda \Lambda\right)}.$$
 (1)

In Eq. 1  $\beta$  is the inverse temperature;  $\mu_i$  are so-called alchemical potentials that are thermodynamically conjugate to the alchemical parameters  $\alpha_i$ , which in this case describe particle shape; N is the number of particles in the system of volume V;  $\Lambda$  is the potential energy function for an Einstein crystal of the target structure;  $\lambda$  is the spring constant of the Einstein crystal; and the sum is taken over particle coordinates and orientations and over the space of particle shapes. Here, we want to satisfy two different system constraints simultaneously. Therefore, following Eq. 1, our combined partition function for the two systems becomes

$$\mathcal{Z} = \int [d\alpha_i] Z(N, \phi_i, T, \alpha_i, \Lambda_1) Z(N, \phi_2, T, \alpha_i, \Lambda_2).$$
 (2)

Using this formalism, we consider two systems, one constrained to structure 1  $(\Lambda_1)$  at density  $\varphi_1$ , and the other constrained to structure 2  $(\Lambda_2)$  at density  $\varphi_2$ . Hard Particle Monte Carlo (MC) simulations using the HPMC module in HOOMD-blue [29,30] translate and rotate particles independently in the two systems. Additionally, following alchemical

MC (Alch-MC) protocols developed for single systems [15,16,31,32], new particle shapes are proposed and either accepted or rejected identically in the two systems according to a single Boltzmann factor. This approach rigorously satisfies detailed balance.

We chose the following nine transitions as our design targets (see Table 1): (1) FCC $\leftrightarrow$ BCC, (2) FCC $\leftrightarrow$  $\beta$ -magnesium cP20-Mn ( $\beta$ -Mn), (3) FCC $\leftrightarrow$  $\gamma$ -Brass cP52-Cu9Al4 ( $\gamma$ -Brass), (4) FCC $\leftrightarrow$  $\beta$ -Tungsten cP8-Cr3Si ( $\beta$ -W), (5) BCC $\leftrightarrow$ SC, (6) BCC $\leftrightarrow$ High Pressure Lithium cI16- Li (cI16), (7) BCC $\leftrightarrow$  $\beta$ -W, (8) BCC $\leftrightarrow$  $\gamma$ -Brass, and (9) FCC $\leftrightarrow$ BCC $\leftrightarrow$ SC. Each of these structures in the nine transitions has been self assembled in simulation [33]. Some of the transitions among the nine can be found in atomic systems, such as FCC $\leftrightarrow$ BCC in iron and steel systems [34], FCC $\leftrightarrow$  $\beta$ -Mn in Ag-Mn systems [35], and BCC $\leftrightarrow$ SC in Ca systems [36], while transitions between structures in colloids have so far only been observed experimentally for FCC $\leftrightarrow$ BCC and BCC $\leftrightarrow$ SC [22–27].

Our protocol consists of two steps. In the first step (design step), we initialised the two systems ( $N \sim 500$ ) in an NVT ensemble with the same randomly generated shape, and slowly compressed each system to its target density  $\varphi = N/V$ , while also performing Alch-MC shape moves. We then relaxed the structural constraints by slowly decreasing  $\lambda$  to zero over  $2 \times 10^7$  MC moves and collected data over another  $2 \times 10^7$  MC moves. In the second step (validation step), we took the particles generated from step one and performed self-assembly runs ( $N \sim 2000$ ) at each target density, and then slowly compressed or expanded the system to confirm the solid–solid phase transition.

For the nine target transitions, we designed particles at several different density differences based on the transition properties. We restricted the particle shapes in four different ways: spheric triangle groups  $\Delta_{332}$  and  $\Delta_{432}$  [28], and randomly generated convex polyhedra with 32 or 64 vertices. Randomly generated convex polyhedra do not admit the simple parametrization of  $\Delta_{332}$  and  $\Delta_{432}$ , so we proposed a new order parameter  $S_l$  (Eq. 5) for particle shape that can quantify its symmetry. The order parameter is computed as follows:

$$S_{ilm} = Y_{lm}(\theta(\overrightarrow{n_i}), \phi(\overrightarrow{n_i})),$$
 (3)

where *i* denotes the *i*-th face of the convex polyhedron,  $\overrightarrow{n_i}$  denotes the normal vector of the *i*-th face, and  $Y_{lm}$  is the spherical harmonic special function.

$$S_{lm} = \sum_{i=1}^{N} A_i S_{ilm},\tag{4}$$

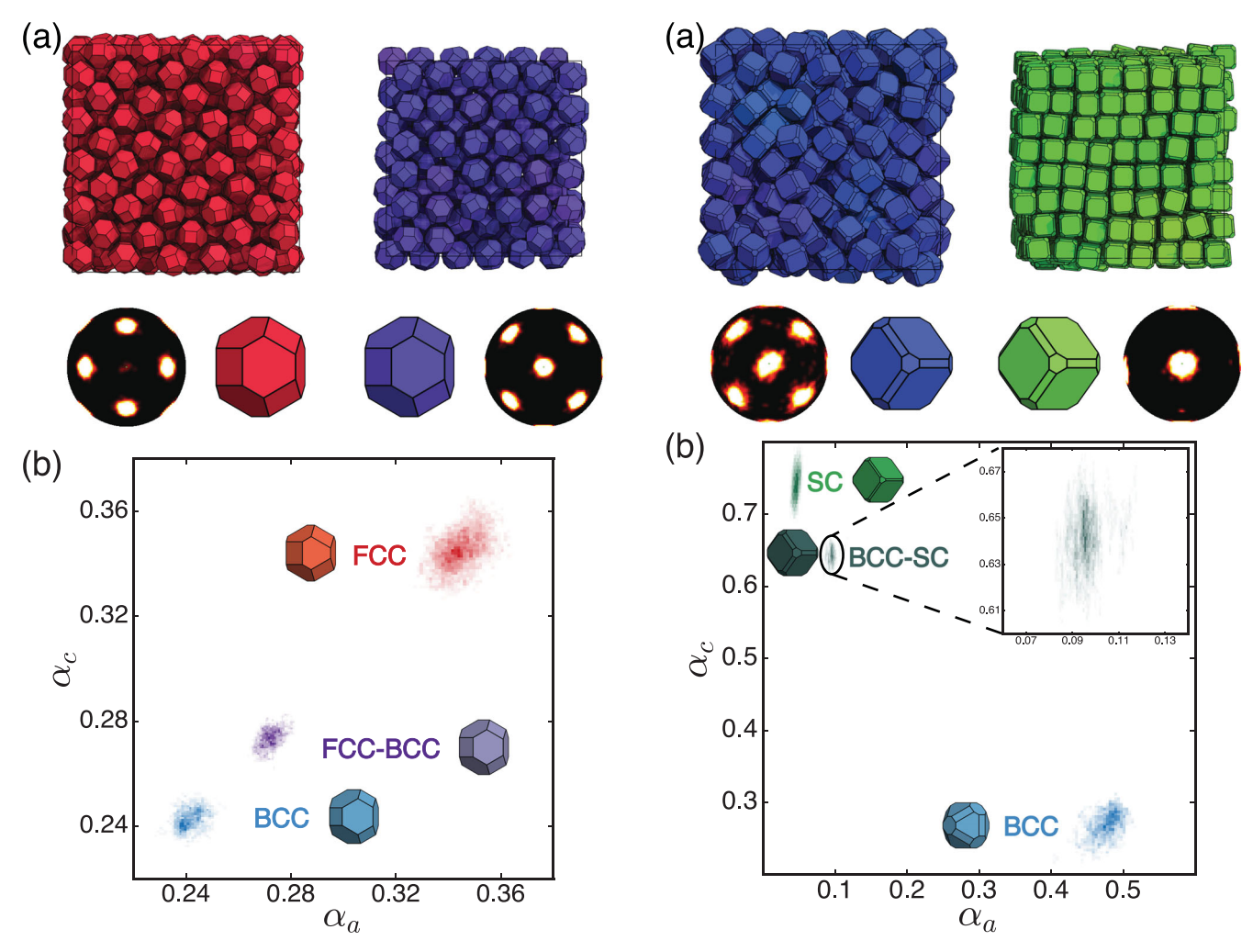


**Figure 2.** (Colour online) (a) Snapshots of the simulation setup: two simulation boxes of structure types FCC (red,  $\varphi=0.55$ ) and BCC (blue,  $\varphi=0.65$ ), bond-orientational order diagrams indicating the structures, and magnified particles to depict their (identical) shape. (b) Heat map for the shape distribution for the optimal FCC shape (red,  $\varphi=0.55$ ), BCC shape (blue,  $\varphi=0.65$ ), and combined shape (purple, with FCC box at  $\varphi=0.55$  and BCC box at  $\varphi=0.65$ ).

**Figure 3.** (Colour online) (a) Snapshots of the simulation setup: two simulation boxes of structure types BCC (blue,  $\varphi=0.55$ ) and SC (green,  $\varphi=0.70$ ), the bond-orientational order diagrams indicating the structures, and magnified particles to depict their (identical) shape. (b) Heat map for the shape distribution for the optimal BCC shape (blue,  $\varphi=0.55$ ), SC shape (green,  $\varphi=0.70$ ), and combined shape (dark green, with BCC box at  $\varphi=0.55$  and SC box at  $\varphi=0.70$ ).

where N denotes the total number of faces of the convex polyhedron and  $A_i$  denotes the area of the i-th face. Since we want the order parameter to be rotationally invariant, we sum over all  $S_{lm}$  values and normalise the result:

$$S_{l} = \left[\frac{4\pi}{2l+1} \sum_{m=-l}^{l} |S_{lm}|^{2}\right]^{1/2}.$$
 (5)

For each transition, we show here for conciseness only results from one type of shape constraint at one density difference, as examples; all other results are included in the Supplementary Information (SI).

#### 3. Results

We grouped the nine transitions into the following three categories: (1) Completely successful, (2) Partially successful, (3) Not successful.

# 3.1. Completely successful

Completely successful means that not only are the two structures stable during the design step even after the external field is removed, but also the density-induced phase transitions occur reversibly during the validation step. The transitions that satisfy both criteria are FCC $\leftrightarrow$ BCC and BCC $\leftrightarrow$ SC. We show results of one example here. Additional examples can be found in the SI.

For FCC $\leftrightarrow$ BCC, all the density differences and shape restrictions we tested were successful. Figure 2 shows the design step result within the  $\Delta_{332}$  shape family with FCC at  $\varphi = 0.55$  and BCC at  $\varphi = 0.65$ . Figure 2(b) shows the particle shape distribution as quantified by the two shape parameters  $\alpha_a$  and  $\alpha_c$  after the systems have equilibrated, for five independent replicas. We also obtained the optimal shape for individual phases FCC and BCC at their respective densities (see Figure 2(b)). The 'combined' optimal shape region is located between the optimal shapes of FCC and BCC, but not equidistant from both optimal shapes. This demonstrates that finding the

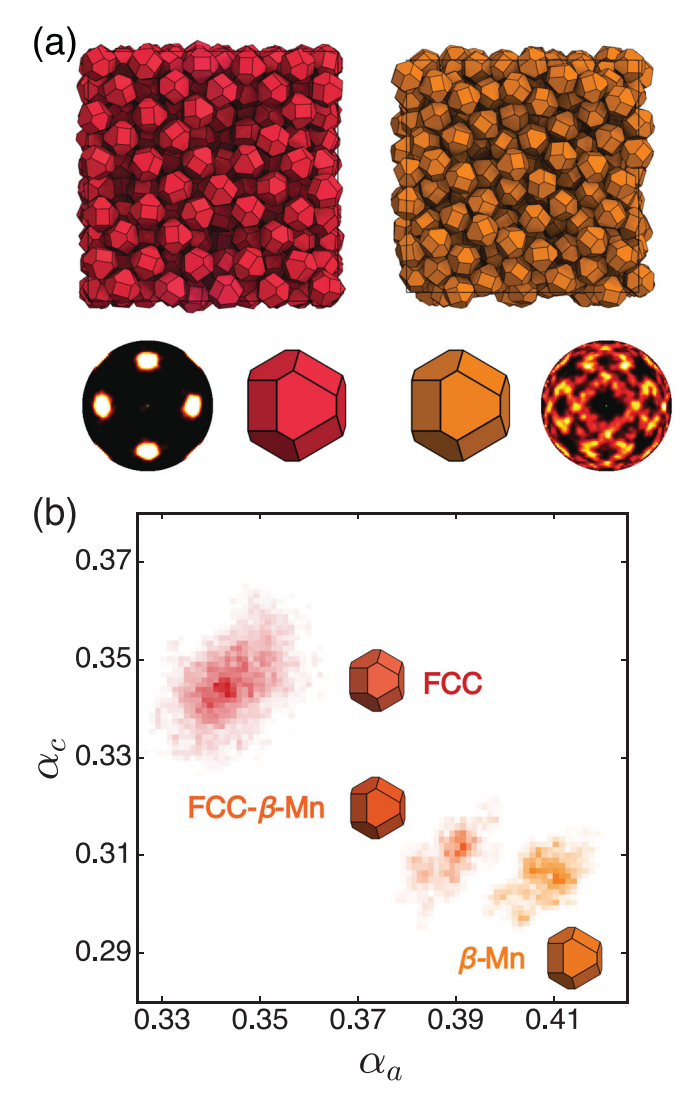


**Figure 4.** (Colour online) (a) Snapshots of the simulation setup: two simulation boxes of structure types FCC (red,  $\varphi=0.55$ ) and  $\beta$ -Mn (orange,  $\varphi=0.60$ ), the bond-orientational order diagrams indicating the structures, and magnified particles to depict their (identical) shape. (b) Heat map for the shape distribution for the optimal FCC shape (red,  $\varphi=0.55$ ),  $\beta$ -Mn shape (orange,  $\varphi=0.60$ ), and combined shape (peach, with FCC box at  $\varphi=0.55$  and  $\beta$ -Mn box at  $\varphi=0.60$ ).

optimal shape for a coupled system is not a matter of simply averaging the two optimal shapes from the two different phases.

During the validation step, we selected the optimal shape and performed two different kinds of validation. First, we initialised the system using the optimal shape arranged into the FCC structure at the lower density, thermalised it, and then slowly compressed the simulation box to the higher density. We observed the phase transition from FCC to BCC and *vice versa*. Second, we initialised the system with the optimal shape in a dense fluid phase. We performed self-assembly runs at the lower density, and observed that the FCC structure self-assembled. We then slowly compressed the simulation box to the higher density and slowly expanded the box to the lower density. Similar to the first validation test, the system transitioned into the BCC structure upon compression and transitioned back into the FCC structure during the expansion process. Detailed analysis and videos of this step can be found in the SI.

For **BCC** $\leftrightarrow$ **SC**, we succeeded in designing shapes within the  $\Delta_{432}$  shape family with BCC at  $\varphi = 0.55$  and SC at  $\varphi = 0.65$  or  $\varphi$ 

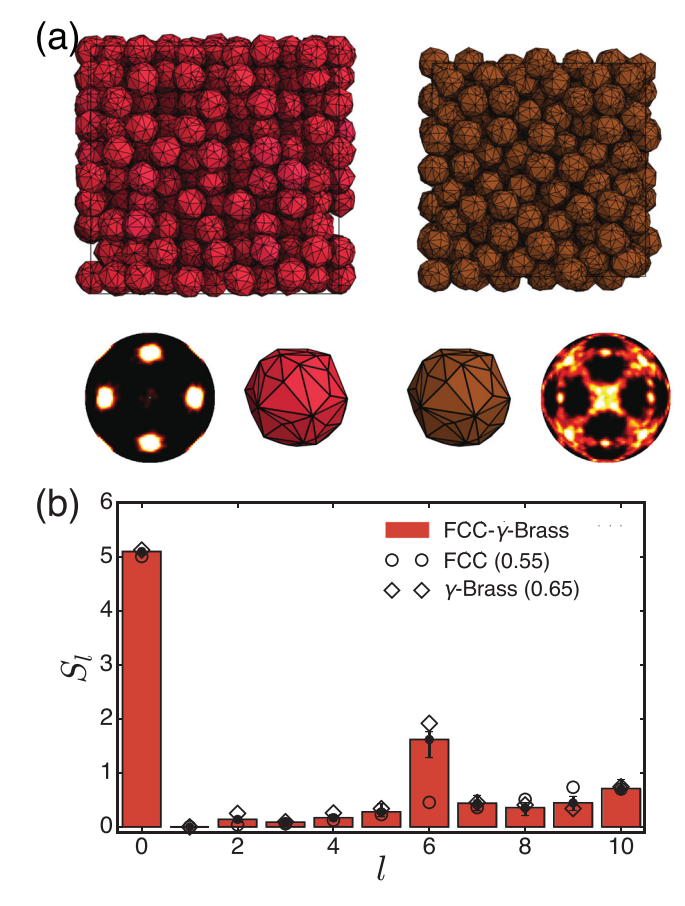


**Figure 5.** (Colour online) (a) Snapshots of the simulation setup: two simulation boxes of structure types FCC (red,  $\varphi = 0.55$ ) and  $\gamma$ -Brass (brown,  $\varphi = 0.65$ ), the bond-orientational order diagrams indicating the structures, and magnified particles to depict their (identical) shape. (b)  $S_I$  analysis for optimal shapes of phase transition FCC $\leftrightarrow \gamma$ -Brass where the two densities are  $\varphi_1 = 0.65$  and  $\varphi_2 = 0.55$ .

= 0.70. Neither the BCC nor SC structures were stable after removing the external field using the other shape restrictions tested. Figure 3 shows the design step result using shape restrictions of the  $\Delta_{432}$  shape family with BCC at  $\varphi = 0.55$  and SC at  $\varphi = 0.70$ . Similar to  $\Delta_{332}$ , shapes in  $\Delta_{432}$  can also be quantified using two shape parameters  $\alpha_a$  and  $\alpha_c$ . In Figure 3(b), we see the shape distribution for both the 'combined' shape, as well as the optimal shape for BCC and SC structures at the two different densities, respectively. Here, though the combined shape still lies in between the optimal shapes for the two structures, it is much closer to the optimal SC shape, unlike in the case of FCC BCC. Again we observe that the optimal combined shape is not as simple as taking the geometric average, because particle shape is a high-dimensional variable, and other structures might assemble in between.

We performed the same validations as described above for FCC↔BCC, and found that the BCC↔SC transition occurs reversibly upon both compression and expansion. Detailed analysis of this transition can be found in the SI.

# 3.2. Partially successful

Whereas FCC 

BCC, and BCC 

SC were found to be thermodynamically stable in Alch-MC simulation and to reversibly transition under compression in MC simulation, for several

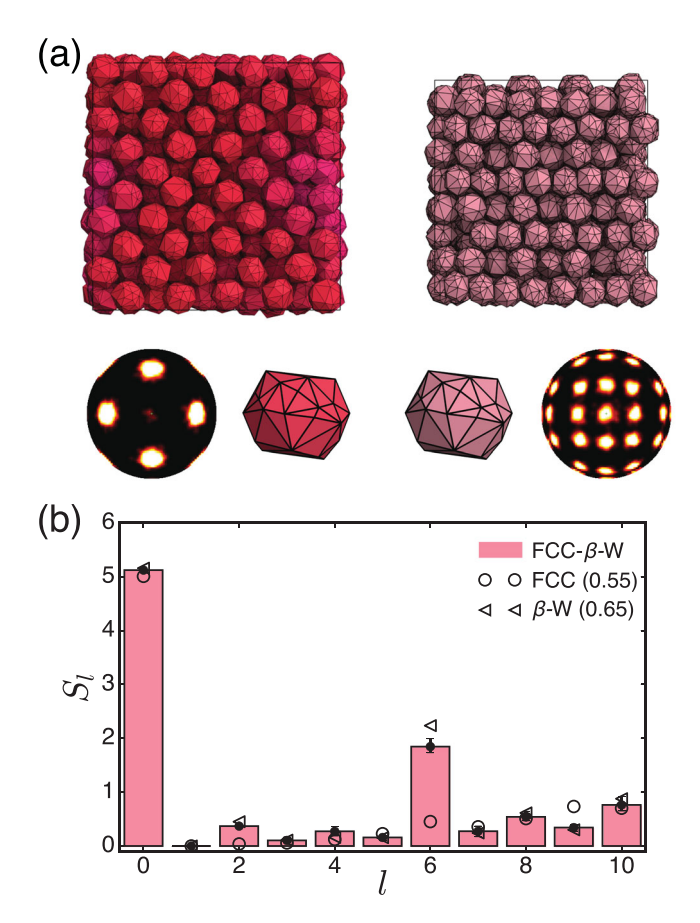


**Figure 6.** (Colour online) (a) Snapshots of the simulation setup: two simulation boxes of structure types FCC (red,  $\varphi=0.55$ ) and  $\beta$ -W (pink,  $\varphi=0.65$ ), the bond-orientational order diagrams indicating the structures, and magnified particles to depict their (identical) shape. (b)  $S_I$  analysis for optimal shapes of phase transition FCC $\leftrightarrow$ β-W where the two densities are  $\varphi_I=0.65$  and  $\varphi_2=0.55$ .

other transitions we found Alch-MC stability but no transition upon compression. Transitions exhibiting this partial success were FCC $\leftrightarrow$  $\beta$ -Mn, FCC $\leftrightarrow$  $\gamma$ -Brass, FCC $\leftrightarrow$  $\beta$ -W and BCC $\leftrightarrow$ cI16.

For  $FCC \leftrightarrow \beta$ -Mn, all shape restrictions and density differences tested were partially successful. Here we show results (see Figure 4) using shape restriction  $\Delta_{332}$  and densities for FCC at  $\varphi = 0.55$  and  $\beta$ -Mn at  $\varphi = 0.60$ . Figure 4(b) shows the convergence of the five different replicas. Despite finding a single shape that thermodynamically optimises two different structures at two different densities, during the validation step we were unable to observe a compression or expansioninduced transformation, so we performed a secondary stability test. We initialised the system ( $N \sim 4000$ ) with half of the particles in the  $\beta$ -Mn structure and the other half in a dense fluid at three different densities  $\varphi$  = 0.55, 0.60, 0.65. After equilibration, we found that at the lower density  $\varphi = 0.55$ , the system became completely FCC, and at higher density  $\varphi = 0.65$ , the system became completely  $\beta$ -Mn. However, at the intermediate density  $\varphi = 0.60$ , we observed that some runs became FCC while the others became  $\beta$ -Mn. This additional test supports our original design solution. Nevertheless, a solid-solid transition was not observed either upon compression or expansion. We interpret this finding as follows: upon compression, the kinetics become restrictive; upon expansion, a transition should be kinetically possible, but evidently is not thermodynamically favoured.

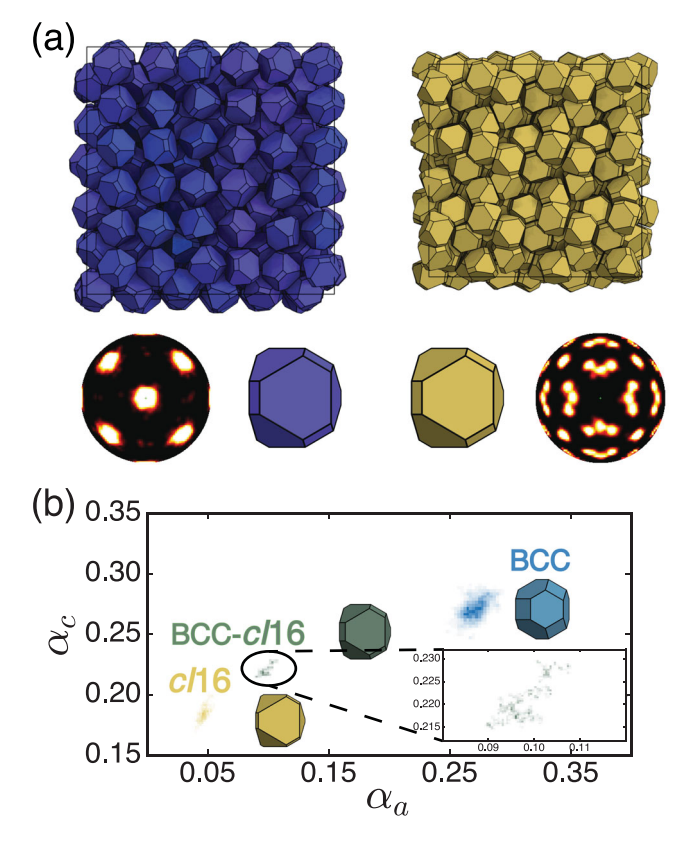


**Figure 7.** (Colour online) (a) Snapshots of the simulation setup: two simulation boxes of structure types BCC (blue,  $\varphi=0.55$ ) and c/16 (yellow,  $\varphi=0.70$ ), the bond-orientational order diagrams indicating the structures, and magnified particles to depict their (identical) shape. (b) Heat map for the shape distribution for the optimal BCC shape (blue,  $\varphi=0.55$ ), c/16 shape (yellow,  $\varphi=0.70$ ), and combined shape (teal, with BCC box at  $\varphi=0.55$  and c/16 box at  $\varphi=0.70$ ).

Since the  $\gamma$ -Brass and  $\beta$ -W structures do not appear in the phase diagram of  $\Delta_{332}$  or  $\Delta_{432}$ , we only used the 32, 64 vertex shape restrictions [16] for **FCC** $\leftrightarrow \gamma$ -**Brass** and **FCC** $\leftrightarrow \beta$ -W transitions. All the density differences tested were stable and Figure 5 shows the result for FCC $\leftrightarrow \gamma$ -Brass while Figure 6 shows the result for FCC $\leftrightarrow \beta$ -W shapes restricted to 64 vertices.

Figures 5(b), and 6(b) show the distribution of the  $S_l$  order parameter. It can be seen in the figures that shapes generated from the different replicas converged to similar symmetry distributions. Circles indicate  $S_l$  of the optimal shape for FCC in both Figures 5(b), 6(b). The triangle and square in Figures 5(b), 6(b) represent  $S_l$  distributions for the optimal shapes of  $\gamma$ -Brass and  $\beta$ -W, respectively. We observe distinct differences in the distribution of the  $S_l$  order parameter for different structures. Also, we notice that similar to the shapes in the shape families, the combined shapes possess symmetry elements of the optimal shapes of the two structures, while favouring slightly the shape optimising the higher density phase.

For neither FCC $\leftrightarrow \beta$ -W nor FCC $\leftrightarrow \gamma$ -Brass, did we observe compression-induced transformation between structures. We again performed secondary stability tests, following the protocol we used for FCC $\leftrightarrow \beta$ -Mn above. We observed all systems transition into FCC for  $\varphi = 0.55$  and  $\beta$ -W for  $\varphi = 0.65$ . For the intermediate density  $\varphi = 0.60$ , we observed coexistence of BCC and  $\beta$ -W. However, for FCC $\leftrightarrow \gamma$ -Brass, all systems became

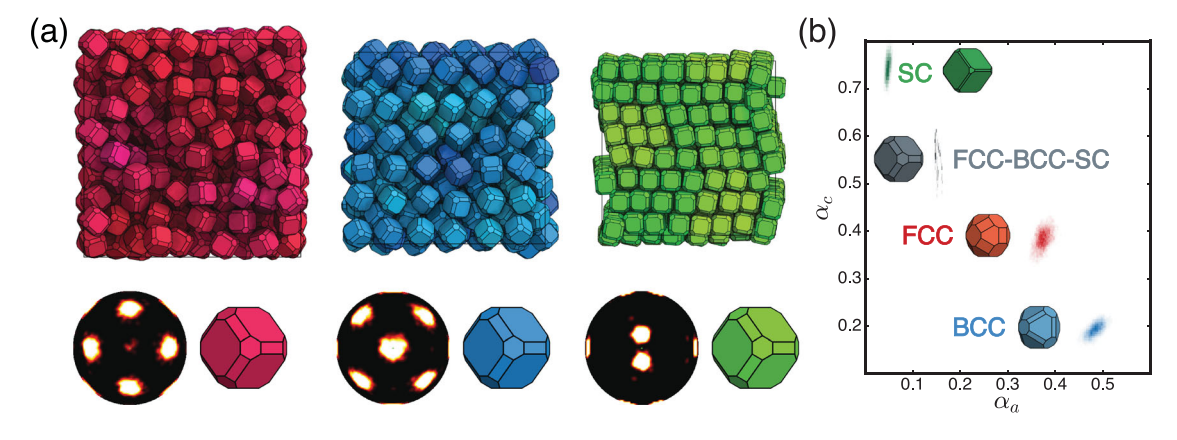


**Figure 8.** (Colour online) (a) Snapshots of the simulation setup: three simulation boxes of structure types FCC (red,  $\varphi=0.55$ ), BCC (blue,  $\varphi=0.60$ ), and SC (green,  $\varphi=0.70$ ), the bond-orientational order diagrams indicating the structures, and magnified particles to depict their (identical) shape. (b) Heat map for the shape distribution for the optimal FCC shape (red,  $\varphi=0.55$ ), BCC shape (blue,  $\varphi=0.60$ ), SC shape (green,  $\varphi=0.70$ ), and combined shape (grey, with FCC box at  $\varphi=0.55$ , BCC box at  $\varphi=0.60$  and SC box at  $\varphi=0.70$ ).

FCC at  $\varphi$  = 0.55 and  $\varphi$  = 0.60, and we observed some growth of  $\gamma$ -Brass at  $\varphi$  = 0.65. The slow growth of the  $\gamma$ -Brass phase can be caused by its big unit cell (52 particles), which could slow down the nucleation process. Among all the structures studied here,  $\gamma$ -Brass has a much bigger unit cell.

For BCC $\leftrightarrow$ cI16, we had some success in all the shape restrictions applied. We found density differences that were stable for both structures for cI16 at  $\varphi = 0.65$ , 0.70 and BCC at  $\varphi = 0.55$ , and for cI16 at  $\varphi = 0.70$  and BCC at  $\varphi =$ 0.60. Figure 7 shows design-step results for shape restriction  $\Delta_{332}$  and BCC at  $\varphi = 0.55$  and cI16 at  $\varphi = 0.70$ . All the independent replicas converged to the same shape parameter range. During the validation step, we found that though it is possible for cI16 to transition into the BCC structure upon expanding the simulation box, the transformation process is not reversible. To test the stability of the cI16 structure using the optimal shape we identified, we initialised the system  $(N \sim 4000)$  with half of the particles in the cI16 structure and the other half in a dense fluid at three different densities  $\varphi = 0.55$ , 0.60, 0.65. After equilibration, we observed that for  $\varphi = 0.55$ , 0.60, all systems transitioned into BCC while for  $\varphi = 0.65$ , some systems transited completely into cI16 while we observed coexistence of BCC and cI16 for some other systems. This result shows that, thermodynamically, cI16 is the more stable phase at higher density. Failure to observe a reversible phase transition could be caused by kinetic constraints.

We also tested the possibility of designing a two-stage solid-solid phase transition. For the two-stage transition, we chose to combine the two completely successful transitions we designed and focused on the shape family  $\Delta_{432}$ , where we had the most success. Figure 8 shows design-step results for a three-way FCC $\leftrightarrow$ BCC $\leftrightarrow$ SC transition. As shown in Figure 8(a), we were able to maintain the structural stability of the three phases, and Figure 8(b) demonstrates that all the shapes converged for the independent replica runs, while being significantly different compared to the results in BCC $\leftrightarrow$ SC (see Figure 3(b)). However, we were not able to observe the two-step solid-solid phase transition during the validation step.

#### 3.3. Not successful

In this category, at least one of the two target structures transformed into some other colloidal crystal structure during the design stage once the design constraint was removed. We mark them as not successful, but this does not mean that these transitions are prohibited for hard particle systems. The BCC structure in transitions  $BCC \leftrightarrow \beta$ -Mn and  $BCC \leftrightarrow \gamma$ -Brass was not found to be stable. Without the external field, all BCC structures transformed into FCC.

# 4. Discussion

In this paper, we showed that extending the 'digital alchemy' framework [15,16,20] to multiple coupled ensembles enables the design of anisotropic colloidal building blocks that exhibit two or three distinct target behaviours under corresponding distinct, pre-specified external conditions. In doing so, we determined particle shapes that undergo density-induced solid-solid transitions in a target density range. Our results demonstrate that it is possible to inversely design building blocks for a target colloidal material function.

We attempted the design of nine sets of transitions and observed reversible transitions between the two phases for two of them (FCC↔BCC, BCC↔SC), for which reversible transitions have been reported [21-27], although we did not observe the same behaviour for five other transitions  $(FCC \leftrightarrow \beta - W,$  $FCC \leftrightarrow \beta$ -Mn, FCC $\leftrightarrow \gamma$ -Brass, BCC $\leftrightarrow$ cI16, FCC↔BCC↔SC) whose target structures are all thermodynamically stable, but for which reversible transitions have not been studied. Though disappointing, this result shows the potential challenges that could arise for inverse design of materials functions (see Figure 9). During the design stage, whether a design protocol is successful or not can be judged very easily by analysing the stability of the crystal structures  $(\Lambda_1, \Lambda_2)$ , or by observing the convergence of the final shape  $(\alpha_1, \alpha_2, \alpha_{12})$ . Among the nine transitions we attempted to design, two transitions failed at this step, which was a direct indicator. However, our method can fail more subtly as we move to the validation step in a few different ways. Digital

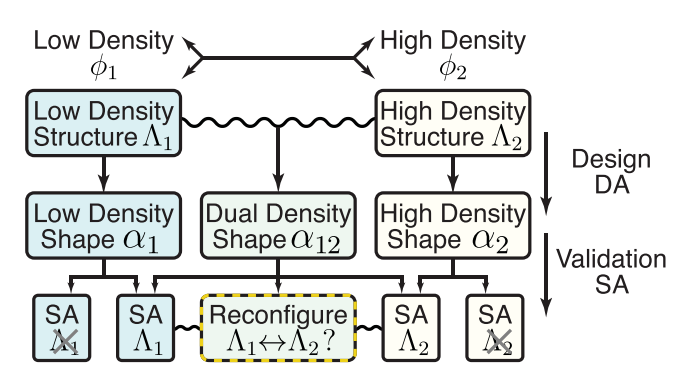


**Figure 9.** Flowchart stating the potential challenges in the inverse design of materials behaviours.

alchemy is based on finding thermodynamic equilibria (*i.e.* finding the desired particle shape for a given set of constraints), which means that we are searching for a target particle shape that minimises the free energy of the system for a given crystal structure and density. However, at the same density, the particle might want to assemble into a different crystal structure that has a lower free energy compared to the one we are designing for or it might prefer a fluid phase. This scenario could already occur when trying to design a particle shape for a single structure, and has a higher chance to appear as we apply more constraints to design a target function.

Moreover, the method does not guarantee that a viable kinetic pathway between the two structures exists, nor does it disfavour metastability for off-target phases. Indeed, recent work has shown that even spontaneous transitions between body-centered structures with two particle unit cells can be strongly suppressed by the form of topological contact between particles at surprisingly low density [37]. Our inability to observe such transitions induced by compression for systems of particles with a constant shape does not imply that those transitions are impossible, but it does suggest other approaches might be required. Such approaches could include more complex forms of structural constraints, e.g. explicitly disfavouring metastability, or employing particle shape change [4,21,38–41].

Although our investigations here focused on designing particle shapes for density-induced reconfiguration in colloids, this approach generalises straightforwardly to, e.g. shape-change-induced transitions [21]. Shape-shifting colloids have been synthesised using a number of techniques such as asymmetric thermal expansion [39], stimulated dewetting [4], and 'colloidal recycling' [41], and we expect that inverse design approaches will be useful in the rational design of functional materials that leverage those synthesis techniques. The approach developed here generalises straightforwardly to problems outside of the domain of materials research to distributed systems [42], and we expect that our methods will be useful in designing reconfigurable distributed systems.

# **Acknowledgements**

We thank J. Proctor, R. Cersonsky, Y. Geng for helpful discussions and encouragement. This material is based upon work supported in part by

the National Science Foundation, Division of Materials Research Award # DMR 1808342, Department of the Navy, Office of Naval Research under ONR award number N00014-18-1-2497 and by a grant from the Si- mons Foundation (256297, SCG). CXD acknowledges a University of Michigan Rackham Predoctoral Fellowship. This work used the Extreme Science and Engineering Discovery Environment (XSEDE), which is supported by the National Science Foundation grant number ACI-1053575, XSEDE award DMR 140129. Additional computational resources and services were supported by Advanced Research Computing at the University of Michigan, Ann Arbor.

# **Disclosure statement**

No potential conflict of interest was reported by the author(s).

#### **Funding**

This work was supported by National Science Foundation: [grant number DMR 1808342]; National Science Foundation: [grant number DMR 140129]; National Science Foundation: [Grant Number ACI-1053575]; Office of Naval Research: [grant number N00014-18-1-2497]; Simons Foundation: [grant number 256297].

#### **ORCID**

Greg van Anders http://orcid.org/0000-0002-9746-2484 Julia Dshemuchadse http://orcid.org/0000-0003-2310-6687

# References

- [1] Manoharan VN. Colloidal matter: packing, geometry, and entropy. Science. 2015;349(6251):1253751–1253751.
- [2] Glotzer SC, Solomon MJ. Anisotropy of building blocks and their assembly into complex structures. Nat Mater. 2007;6(8):557–562.
- [3] Sacanna S, Pine DJ. Shape-anisotropic colloids: building blocks for complex assemblies. Curr Opin Colloid Interface Sci. 2011;16 (2):96–105.
- [4] Youssef M, Hueckel T, Yi G-R, et al. Shape-shifting colloids via stimulated dewetting. Nat Commun. 2016;7:12216.
- [5] Gong Z, Hueckel T, Yi G-R, et al. Patchy particles made by colloidal fusion. Nature. 2017;550(7675):234–238.
- [6] Wang Y, Wang Y, Breed DR, et al. Colloids with valence and specific directional bonding. Nature. 2012;491(7422):51–55.
- [7] Zhang Y, Lu F, van der Lelie D, et al. Continuous phase transformation in nanocube assemblies. Phys Rev Lett. 2011;107(13):135701.
- [8] Lu F, Yager KG, Zhang Y, et al. Superlattices assembled through shape-induced directional binding. Nat Commun. 2015;6(1):6912.
- [9] Wang Y, McGinley JT, Crocker JC. Dimpled polyhedral colloids formed by colloidal crystal templating. Langmuir. 2017;33 (12):3080–3087.
- [10] McGinley JT, Wang Y, Jenkins IC, et al. Crystal-templated colloidal clusters exhibit directional DNA interactions. ACS Nano. 2015;9 (11):10817–10825.
- [11] Young KL, Personick ML, Engel M, et al. A Directional entropic force approach to assemble anisotropic nanoparticles into superlattices. Angew Chem Int Ed. 2013;52:13980–13984.
- [12] Lin H, Lee S, Sun L, et al. Clathrate colloidal crystals. Science. 2017;355(6328):931–935.
- [13] Henzie J, Grünwald M, Widmer-Cooper A, et al. Self-assembly of uniform polyhedral silver nanocrystals into densest packings and exotic superlattices. Nat Mater. 2012;11(2):131–137.
- [14] van Anders G, Klotsa D, Ahmed NK, et al. Understanding shape entropy through local dense packing. Proc Natl Acad Sci USA. 2014;111(45):E4812–E4821.
- [15] van Anders G, Klotsa D, Karas AS, et al. Digital alchemy for materials design: colloids and beyond. ACS Nano. 2015;9 (10):9542–9553.

- [16] Geng Y, van Anders G, Dodd PM, et al. Engineering entropy for the inverse design of colloidal crystals from hard shapes. Sci Adv. 2019;5:
- [17] Jain A, Errington JR, Truskett TM. Dimensionality and design of Isotropic interactions that stabilize honeycomb, square, simple cubic, and diamond lattices. Physical Review X. 2014;4(3):031049.
- Lindquist BA, Jadrich RB, Piñeros WD, et al. Inverse design of selfassembling Frank-Kasper phases and insights into emergent quasicrystals. J Phys Chem B. 2018;122(21):5547-5556.
- [19] Adorf CS, Antonaglia J, Dshemuchadse J, et al. Inverse design of simple pair potentials for the self-assembly of complex structures. J Chem Phys. 2018;149(20):204102.
- [20] Zhou P, Proctor JC, van Anders G, et al. Alchemical molecular dynamics for inverse design. Mol Phys. 2019;1:3968-3980.
- [21] Du CX, van Anders G, Newman RS, et al. Shape-driven solid-solid transitions in colloids. Proc Natl Acad Sci USA. 2017;114(20): E3892-E3899.
- [22] Qi W, Peng Y, Han Y, et al. Nonclassical nucleation in a solid-solid transition of confined hard spheres. Phys. Rev. Lett.. 2015;115 (18):185701.
- [23] Yethiraj A, Wouterse A, Groh B, et al. Nature of an electric-fieldinduced colloidal martensitic transition. Phys Rev Lett. 2004;92 (5):058301.
- [24] Peng Y, Wang F, Wang Z, et al. Two-step nucleation mechanism in solid-solid phase transitions. Nat Mater. 2015;14(1):101-108.
- Mohanty PS, Bagheri P, Nöjd S, et al. Multiple path-dependent routes for phase-transition kinetics in thermoresponsive and fieldresponsive ultrasoft colloids. Physical Review X. 2015;5(1):011030.
- [26] Casey MT, Scarlett RT, Benjamin Rogers W, et al. Driving diffusionless transformations in colloidal crystals using DNA handshaking. Nat Commun. 2012;3(1).
- [27] Zhang Y, Pal S, Srinivasan B, et al. Selective transformations between nanoparticle superlattices via the reprogramming of DNA-mediated interactions. Nat Mater. 2015;14(8):840-847.
- [28] Chen ER, Klotsa D, Engel M, et al. Complexity in surfaces of densest packings for families of polyhedra. Physical Review X. 2014;4(1):011024.

- [29] Anderson JA, Lorenz CD, Travesset A. General purpose molecular dynamics simulations fully implemented on graphics processing units. J Comput Phys. 2008;227(10):5342-5359. http://codeblue. umich. edu/hoomd- blue.
- Anderson JA, Irrgang ME, Glotzer SC. Scalable metropolis Monte Carlo for simulation of hard shapes. Comp Phys Commun. 2016;204:21-30.
- Cersonsky R, van Anders G, Dodd PM, et al. Relevance of packing to colloidal self-assembly. Proc Natl Acad Sci USA. 2018;115(7):1439-
- [32] Geng Y, van Anders G, Glotzer SC. Predicting colloidal crystals from shapes via inverse design and machine learning, arXiv Preprint ArXiv. 2018: 1801.06219.
- [33] Damasceno PF, Engel M, Glotzer SC. Predictive self-assembly of polyhedra into complex structures. Science. 2012;337(6093):453-457.
- Porter DA. Phase transformations in metals and alloys. 3rd ed. Florida: CRC Press; 2009.
- [35] Karakaya I, Thompson W. The Ag-Mn (Silver-Manganese) system. J Phase Equilibr. 1990;11(5):480-486.
- [36] Olijnyk H, Holzapfel W. Phase transitions in alkaline earth metals under pressure. Phys Lett A. 1984;100(4):191-194.
- Zygmunt W, Teich EG, van Anders G, et al. Topological order in densely packed anisotropic colloids. Phys Rev E. 2019;100:032608.
- Gang O, Zhang Y. Shaping phases by Phasing shapes. ACS Nano. 2011;5:8459.
- Lee KJ, Yoon J, Rahmani S, et al. Spontaneous shape reconfigurations in multicompartmental microcylinders. Proc Natl Acad Sci. 2012;109(40):16057-16062.
- Zhou J, Turner SA, Brosnan SM, et al. Shapeshifting: reversible shape memory in semicrystalline elastomers. Macromolecules. 2014;47 (5):1768-1776.
- [41] Meester V, Verweij RW, van der Wel C, et al. Colloidal recycling: reconfiguration of random aggregates into patchy particles. ACS Nano. 2016;10(4):4322-4329.
- Klishin AA, Shields CP, Singer DJ, et al. Statistical physics of design. New J Phys. 2018;20(10):103038.